Automated Concrete Crack Inspection with Directional Lighting Platform

Jack McAlorum[1], Hamish Dow[1], Sanjeetha Pennada[1], Marcus Perry[1] and Gordon Dobie[2]
[1]*Department of Civil and Environmental Engineering, University of Strathclyde, Glasgow, G1 1XJ, UK*
[2]*Department of Electronic and Electrical Engineering, University of Strathclyde, Glasgow, G1 1XW, UK*

Manuscript received Sep 15, 2023; revised June 21, 2017; accepted July 6, 2017. Date of publication July 12, 2017; date of current version July 12, 2017.

Abstract—This paper presents the development and performance evaluation of a novel platform for visual concrete crack inspection. Concrete surfaces are imaged using directional lighting to support accurate crack detection, classification and segmentation. In addition to developing lab- and field- deployable hardware iterations, we outline customised convolutional neural networks and filters that leverage the directionally-lit data set. Crack classification and segmentation accuracies were both 10% higher than accuracies for standard imaging techniques with diffuse lighting, and crack widths of 0.1 mm were reliably detected and segmented. The major innovation described here is the combination of new hardware platforms for directional lighting, with a suite of algorithms that utilise the directionally-lit data set to improve crack detection and evaluation. This work demonstrates that directional lighting can improve the performance and robustness of automated concrete inspection. This could be key in supporting the efforts of asset managers as they seek to automate inspections of their ageing populations of concrete assets.

Index Terms—concrete inspection, visual inspection, crack detection, geometrical illumination, robotic inspection

I. INTRODUCTION

Routine visual inspections of concrete structures can pose risks to inspectors' health and wellbeing, delay projects, disrupt asset use, and lead to low inspection repeatability. Automated inspection and deep learning could provide asset managers with remote and traceable tools to uphold concrete structural health and resilience [1]–[3], but many automated systems still lack the adaptability to assess diverse defects under varying and uncontrolled lighting conditions.

In this paper, we present the development and testing of a new image acquisition and analysis platform called ALICS (Adaptive Lighting for the Inspection of Concrete Structures). ALICS can be used as a hand-held device to support documentation, or it can be mounted to robots or vehicles to support semi-automated crack inspection. The platform uses directional lighting to enhance the detection, classification, and segmentation of concrete cracks.

Directional lighting has been used to enhance feature contrast during surgery [4], and on production lines [5]. The use of illumination has been only briefly explored in the context of civil structures. Authors in [6] used angled lighting to highlight concrete textural differences, but found that this reduced the accuracy of crack detection neural networks, as the models were trained on images lit using standard diffuse lighting. Authors in [7] and [8] analysed the impact of brightness and lighting direction on void detection, and found that low-intensity, low-angle lighting supported smaller feature detection.

There are currently a lack of image processing algorithms that are trained on data sets comprised of directionally-lit images. The work presented in this paper is, to our knowledge, the first demonstration of the automation of directional lighting for concrete crack image acquisition and the first demonstration of convolutional neural networks and filters that fully leverage the directionally-lit data set to ehance crack identification and segmentation.

Corresponding author: M. Perry (e-mail: m.perry@strath.ac.uk).

Associate Editor: X.
Digital Object Identifier 10.1109/LSENS.2017.0000000

II. HARDWARE DEVELOPMENT

A. Machine vision set up

In this work, a FLIR Blackfly 1" sensor machine vision camera was used with the parameters outlined in Table 1. These settings allowed images to be taken with a spatial resolution of 0.1 mm/pixel, a field of view of approx 500 mm × 350 mm, and an exposure time of 0.2 seconds. The concrete surface could be imaged with clarity at working distances between 200 mm and 450 mm, with no discernible diffraction effects, and with acceptable levels of edge blurring.

To account for lens image distortion, images of checkerboard patterns at various distances and angles were captured. Distortion correction coefficients were calculated using a checkerboard pattern and applied using Python's OpenCV camera calibration module.

B. Lighting hardware

Directional lighting presented a new parameter space that required exploration so that we could optimise the lighting configuration for imaging concrete faults. To this end, we developed the lab-based rig shown in Figure 1a). The machine-vision camera is surrounded by four 3-jointed servo-motorized arms holding LED strips. This allows scenes to be lit from the up (U), down (D), left (L), or right (R) direction, or any combination of these directions (e.g. UD, UDL), including diffuse illumination by lighting from all directions at once (all, A=UDLR). Each arm can project light at angles incident to the surface ranging from θ_L = 5° to 50° and at various proximities to the concrete surface. This rig was mounted to a six-axis robot so that we could automate the scanning of large concrete surfaces in a dark room. Illuminance in the room during testing was 0.2 lux.

C. Lab data set acquisition

Three-point bending loads of magnitude 700 N were applied to the faces of unpolished, reinforced concrete slabs of size 600 mm × 600 mm × 20 mm to produce tensile cracks. Slabs were flattened

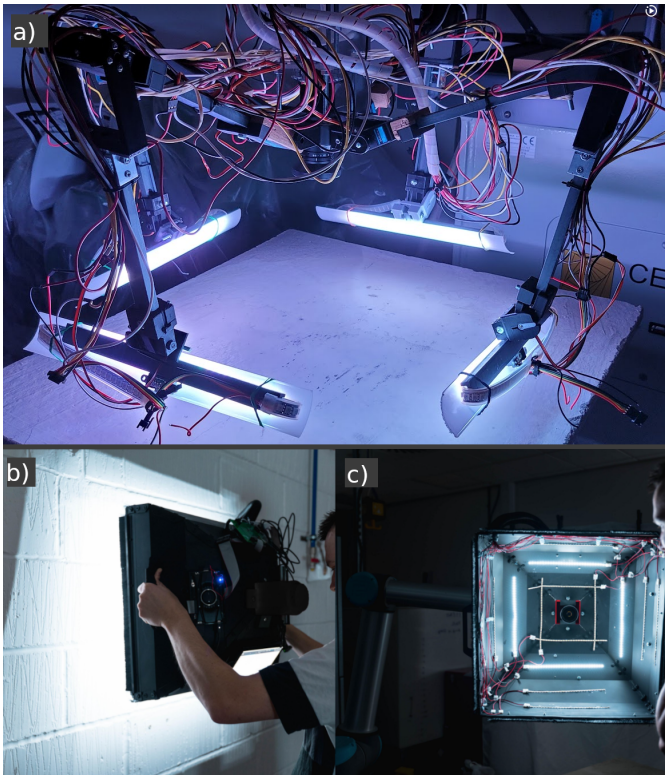

Fig. 1. a) Lab rig used to explore the lighting parameter space; and field-deployable rig shown: b) as a handheld device, and; c) mounted to a six-axis robot.

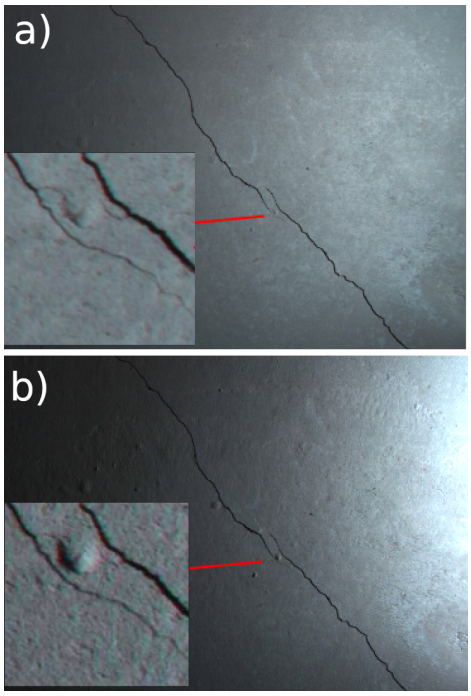

Fig. 2. Slab area lit from the right, R, at angles: a) $\theta_L = 50^\circ$, and; b) $\theta_L = 10^\circ$. Inset images show the same 224 × 224 pixel block.

TABLE 1. Lens and camera parameters.

Parameter	Variable	Value
Aperture diameter	a_d	1 mm
Focal length	f	8 mm
Working distance	D	300 mm
f-number	$N = f/a_d$	8
Circle of confusion	$c \approx d/1500d$	11 µm
Depth of field	$DOF = \frac{2D^2Nc}{f^2}$	250 mm

after bending to obtain thinner crack widths. To vary the location of the cracks, bending support positions were changed for each slab. Branching cracks were random in orientation, and ranged from 0.1 – 1 mm wide, and 10 mm to 500 mm long. The summed area of all slabs in the lab was approx 2 m^2, allowing us to capture 12 distinct 500 mm × 350 mm images that were manually annotated to produce ground truths for benchmarking image processing algorithm accuracy.

An example slab under varying lighting conditions is shown in Figure 2. Inset images show a 224 × 224 pixel block (equivalent to a 20 mm × 20 mm area on the slab). The figure shows that concrete surface roughness becomes more apparent at lower lighting angles.

D. Field-deployable rig

Lab results outlined in Section IV allowed us to commit to specific lighting angles and develop a second more robust iteration of the ALICS imaging platform shown in Figures 1b) and 1c). The device comprises a lightweight aluminium shroud to block ambient light, LED strips to provide illumination at fixed angles, and a machine vision camera at the apex of the shroud facing the concrete surface. For an outdoor illuminance of 6000 lux (daylight conditions), illuminance under the shroud was 0.2 lux. This rig was used to acquire a limited number of field data sets from concrete assets in public areas.

III. IMAGE PROCESSING DEVELOPMENT

Image based crack detection, classification, and segmentation can be achieved using black-box techniques, such as convolutional neural networks (CNNs) [9], or white-box techniques, such as thresholding and filter-based edge-detection [10]. In this work, we opted for a hybrid black-/white- box approach described as follows:

1) A faster region-based convolutional neural network (Faster R-CNN) detects and roughly locate cracks against the background of undamaged concrete using bounding boxes.
2) The area within the bounding boxes is segmented into 224 × 224 pixel blocks. A VGG-16 CNN is run on each block within the bounding box to more accurately localize and classify cracks.
3) White-box techniques are used on the blocks labelled as positive by VGG-16 to segment cracked pixels within each block. Binary images are then stitched back together.

Through extensive testing, it was found that the only lighting configurations needed to improve crack inspection were U, D, L, R and A at a fixed angle of θ_L=50°. This may not necessarily be the case for all algorithms or for other concrete faults and for wider cracks. The following subsections provide more detailed descriptions of each step, and the results of benchmarking on lab data sets.

A. Faster R-CNN feature detection

Two-shot region-based CNNs (R-CNNs) consist of a region proposal network (RPN), which detects features of interest against a background, followed by a CNN classifier network. The R-CNN used in this work was Tensorflow's Faster-R-CNN Inception v2 COCO, trained via transfer learning on 400 manually-annotated publicly-available concrete crack images [11]. Training images were all captured under diffuse or ambient lighting conditions.

In this work, Faster R-CNN used the diffused image (A) only to detect and locate cracks on the surface. The Area Under Curve, AUC, of the Precision-Recall plot was used to assess the accuracy of the R-CNN under various values of θ_L. It was found that angles of θ_L = 10, 20, 30 ° produced mean AUC values of 0.5 across all of our samples, as shallow lighting angles accentuate surface texture, and the edges of these features can erroneously be picked up as cracks. Values of θ_L = 40 and 50 ° produced mean AUC values of 0.7.

B. VGG-16 classifier

VGG-16 has been used successfully for crack detection in several studies including [12]. The objective of the VGG-16 model in this work was to filter 224 × 224 blocks within the bounding box obtained from R-CNN into binary categories (cracked=1, uncracked=0). R-CNN downselects cracked regions of the image prior to VGG-16 as this reduces the computation time of running VGG-16 on all blocks.

Transfer learning was used to train the VGG-16 model on an extensive data set gained from both our directional lighting apparatus and publicly available crack data [11]. Dropout was added to mitigate overfitting, and a dense layer with sigmoid activation supported binary classification. We adopted a trial-and-error approach to configure network parameters, using the Adam optimizer with binary cross-entropy loss and accuracy metrics. The model underwent 10 epochs of training (batch size 32), with final evaluation on testing data.

In lab testing on ground-truthed images, VGG-16 accuracy (the ratio of true positives and true negatives to all classifications) was found to be highest (98%) for lighting angles of θ_L = 50 °. This was an improvement of 10% over diffused lighting for our particular data set, and provides further support for the use of this angle. This accuracy is high, but should be interpreted with caution as these are initial tests on a limited lab data set. It is the 10% improvement in accuracy when using directional lighting that is the main result, rather than the absolute accuracy value. The network's performance in the face of noise and blurring is discussed in our other work[13].

C. White-box segmentation

The white-box segmentation algorithm only recieves 224 × 224 pixel blocks labelled as cracked by the VGG-16 classifier. This improves the robustness and accuracy of the segmentation, as other features (marks on the surface) are pre-filtered by the classifier. This reduces the overall number of false positive pixels.

Figure 3 illustrates the white-box method used in this work. Images lit from U, D, L and R were combined with the diffused image (A) to enhance crack contrast. Edges were detected in each image using a 3 × 3 pixel Laplacian kernel, producing four binary masks that were combined using a bitwise OR operation. In the final image, positive pixels remain if they were positive in at least one input image. Following this process, segmented cracks are joined, and noise is removed using the skele-marker method described in our previous work [14]. During benchmarking, it was found that the Dorafshan white-box method [15] achieved a 54% accuracy in predicting crack pixels on diffused images, whereas the bitewise OR combination of directionally lit images achieved a 69% accuracy.

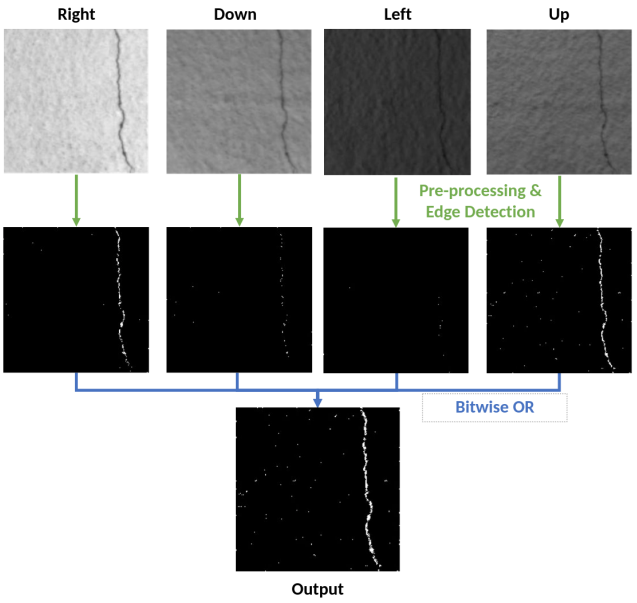

Fig. 3. Directionally-lit image combination using white-box method.

IV. RESULTS AND DISCUSSION

Figure 4 shows example and sequential outputs for each step in our algorithm on a lab sample: a) Faster R-CNN draws bounding boxes around two features labelled as cracks; b) VGG-16 classifies blocks within those bounding boxes; c) the white-box algorithm segments the cracked pixels. Segmentation image contrast has been enhanced for the sake of visibility in this paper; this crack is on average 0.1 mm wide or less. Surface markings and uneven surfaces in the top left and bottom left of this image may have posed a challenge for the white-box segmenter, but have have been filtered out by the R-CNN.

VGG-16 leverages the directionally lit data set to filter out uncracked blocks with a higher accuracy at a higher computation cost. False positives from the R-CNN bounding box on the left, the result of an uneven casting surface, are discarded by VGG-16. VGG-16 is currently needed to fully leverage the directionally lit data set, but there will be future work required to assess other CNNs and better integrate them as the classifier networks of Faster R-CNN.

Example outputs of the algorithm on field data set images are shown in Figure 5. VGG-16 crack classification accuracies were 89% on the field data set. This is a 10% drop relative to the lab data set, owing to the fact that real concrete structures are more varied than the lab data set, and contain significantly more crack types and surface textures. The field data set is still relatively small at this stage, and future work will look to improve accuracy and robustness by training the CNN on broader fault types in the face of confounding variables linked surface paints, effloresence and biofouling.

Images in Figures 5 a), b), c) were classified as containing cracks. The segmentation's binary mask is shown as blue pixels overlaid on the images. The white-box algorithm has generally performed well,

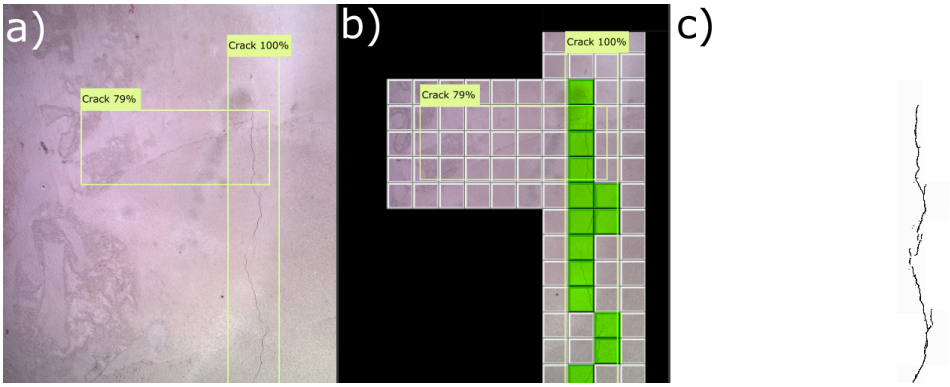

Fig. 4. Overview of the outputs from a) Faster R-CNN, b) VGG-16 and c) the white-box segmentation algorithm. The white-box output's image contrast has been enhanced for clarity.

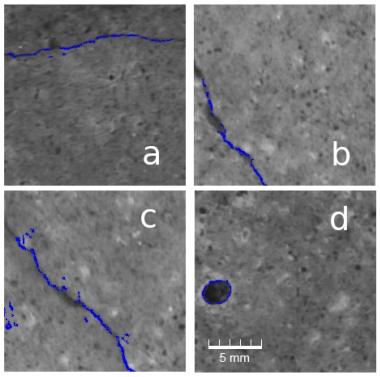

Fig. 5. Four example outputs of the white-box segmentation algorithm on the field data set with overlaid binary masks.

but still contains noise (e.g. see image c). Cracks in images range from 0.07 mm to 0.3 mm and have all been segmented successfully. The algorithms described in this paper can reliably detect and segment 0.1 mm cracks, and can often pick out features below this level. In image b, the algorithm has failed to segment cracks that are significanly wider than those contained in the lab data set. Future work will therefore look to further improve the robustness of this algorithm by tuning the pre-processing steps and the edge-detection methods. Image d in Figure 5 shows that the white-box algorithm has detected and segmented exposed aggregate. The VGG-16 CNN did not classify this block as containing a crack, so it would not be flagged as a fault to be segmented, but it has been included here to demonstrate how using a hybrid black-/white- box approach can reduce overall false positive rates.

V. CONCLUSIONS

This paper presented the design and assessment of an automated hardware and software platform for the directional lighting of concrete surfaces to improve crack detection rates. In lab studies, lighting at a 50° angle was found to improve detection and classification rates for cracks in concrete faces. These lab studies and benchmarks supported the production of a second, more robust hardware iteration, that faciliated the demonstration of concrete crack detection and segmentation in the field. Future work will look to increase the volume and breadth of this field data set, investigate the platform's robustness when imaging various and concurrent defects, and evaluate other neural network architectures with directional lighting.

ACKNOWLEDGMENT

This work was funded in part by the Scottish Funding Council and the University of Strathclyde's Advanced Nuclear Research Centre.

REFERENCES

[1] C. Koch, S. G. Paal, A. Rashidi, Z. Zhu, M. König, and I. Brilakis, "Achievements and challenges in machine vision-based inspection of large concrete structures," *Advances in Structural Engineering*, vol. 17, no. 3, pp. 303–318, 2014.

[2] Y. Yu, M. Rashidi, B. Samali, M. Mohammadi, T. N. Nguyen, and X. Zhou, "Crack detection of concrete structures using deep convolutional neural networks optimized by enhanced chicken swarm algorithm," *Structural Health Monitoring*, vol. 21, no. 5, pp. 2244–2263, 2022.

[3] Y. Yu, B. Samali, M. Rashidi, M. Mohammadi, T. N. Nguyen, and G. Zhang, "Vision-based concrete crack detection using a hybrid framework considering noise effect," *Journal of Building Engineering*, vol. 61, p. 105246, 2022.

[4] J. Shen, H. Wang, Y. Wu, A. Li, C. Chen, and Z. Zheng, "Surgical lighting with contrast enhancement based on spectral reflectance comparison and entropy analysis," *Journal of Biomedical Optics*, vol. 20, no. 10, pp. 1 – 7, 2015.

[5] V. Elango and L. Karunamoorthy, "Effect of lighting conditions in the study of surface roughness by machine vision," *The International Journal of Advanced Manufacturing Technology*, vol. 37, no. 1, pp. 92–103, Apr 2008.

[6] Z. Chen, R. Derakhshani, C. Halmen, and J. Kevern, "A texture-based method for classifying cracked concrete surfaces from digital images using neural networks," *International Joint Conference on Neural Networks*, pp. 2632–2637, 07 2011.

[7] H.-W. Cho, H.-J. Yoon, and J.-C. Yoon, "Analysis of crack image recognition characteristics in concrete structures depending on the illumination and image acquisition distance through outdoor experiments," *Sensors*, vol. 16, no. 10, 2016.

[8] Y. Wei, Z. Wei, K. Xue, W. Yao, C. Wang, and Y. Hong, "Automated detection and segmentation of concrete air voids using zero-angle light source and deep learning," *Automation in Construction*, vol. 130, p. 103877, 2021.

[9] A. Müller, N. Karathanasopoulos, C. C. Roth, and D. Mohr, "Machine learning classifiers for surface crack detection in fracture experiments," *International Journal of Mechanical Sciences*, vol. 209, p. 106698, 2021.

[10] H. S. Munawar, A. W. A. Hammad, A. Haddad, C. A. P. Soares, and S. T. Waller, "Image-based crack detection methods," *Infrastructures*, vol. 6, no. 8, 2021.

[11] C. Ozgenel, "Performance comparison of pretrained convolutional neural networks on crack detection in buildings," *Automation and Robotics in Construction*, 2019.

[12] Z. Qu, J. Mei, L. Liu, and D.-Y. Zhou, "Crack detection of concrete pavement with cross-entropy loss function," *IEEE Access*, 03 2020.

[13] S. Pennada, M. Perry, H. Dow, and G. Dobie, "Threshold-based brisque-assisted deep learning for enhancing crack detection in concrete structures," *MDPI J. Imaging*, vol. in print, no. X, p. X, 2023.

[14] H. Dow, M. Perry, J. McAlorum, S. Pennada, and G. Dobie, "Skeleton-based noise removal algorithm for binary concrete crack image segmentation," *Automation in Construction*, vol. 151, p. 104867, 2023.

[15] S. Dorafshan, R. J. Thomas, and M. Maguire, "Comparison of deep convolutional neural networks and edge detectors for image-based crack detection in concrete," *Construction and Building Materials*, vol. 186, pp. 1031–1045, 2018.